Effective Hamiltonian based Monte Carlo for the BCS to BEC crossover in the attractive Hubbard model

Kanika Pasrija,[1] Prabuddha B. Chakraborty,[2] and Sanjeev Kumar[1]
[1]*Indian Institute of Science Education and Research Mohali, Sector 81, S.A.S. Nagar, Manauli 140306, India*
[2]*Indian Statistical Institute, Chennai Centre, SETS Campus, MGR Knowledge City, Taramani, Chennai 600113, India*
(Received 30 May 2016; revised manuscript received 30 September 2016; published 21 October 2016)

We present an effective Hamiltonian based real-space approach for studying the weak-coupling BCS to the strong-coupling Bose-Einstein condensate crossover in the two-dimensional attractive Hubbard model at finite temperatures. We introduce and justify an effective classical Hamiltonian to describe the thermal fluctuations of the relevant auxiliary fields. Our results for T_c and phase diagrams compare very well with those obtained from more sophisticated and CPU-intensive numerical methods. We demonstrate that the method works in the presence of disorder and can be a powerful tool for a real-space description of the effect of disorder on superconductivity. From a combined analysis of the superconducting order parameter, the distribution of auxiliary fields, and the quasiparticle density of states, we identify the regions of metallic, insulating, superconducting, and pseudogapped behavior. Our finding of the importance of phase fluctuations for the pseudogap behavior is consistent with the conclusions drawn from recent experiments on NbN superconductors. The method can be generalized to study superconductors with nontrivial order-parameter symmetries by identifying the relevant auxiliary variables.

DOI: 10.1103/PhysRevB.94.165150

I. INTRODUCTION

The attractive Hubbard model (AHM) is the standard phenomenological model that describes the transition from a high-temperature metallic or insulating state to a low-temperature superconducting state [1,2]. While the microscopic description requires an explanation for the origin of the effective attraction between electrons [3,4], the nature of the thermally driven transition can be understood within the attractive Hubbard framework. Furthermore, the desired symmetry of the superconducting order parameter can be realized by appropriate choice of the attractive interactions; e.g., an on-site attraction leads to s-wave pairing, a nearest-neighbor (nn) attraction gives rise to d-wave pairing, and a next-nn attraction in a two orbital model can describe s^{+-} and s^{++} symmetry [5–7]. More recently, the AHM has also been used to identify topological quantum phase transitions [8].

In the limit of weak coupling, the AHM can be studied within the BCS mean-field theory, and it provides a complete understanding of the thermally driven transition, and an accurate prediction for the transition temperatures. The mean-field theory, however, fails in the strong-coupling limit where the transition is controlled by phase fluctuations. Indeed, an effective XY model for phase fluctuations is used to describe the physics of the strong-coupling superconductivity [9,10]. This strong-coupling limit is also known as the Bose-Einstein condensate (BEC) limit where the superconducting phase is understood as a condensate of preformed Cooper pairs. To describe the crossover from the weak-coupling BCS to the strong-coupling BEC limit within a single framework is a challenging problem. Various state-of-the-art methods have been employed to gain insight into the behavior of the superconductor (SC) across the BCS to BEC crossover [11–21]. The problem becomes even more challenging in the presence of impurities, which are always present in materials [22–24]. In fact, disorder as a control parameter has become a powerful concept in understanding some fundamental aspects of superconductivity. Recent discovery of a Higgs mode in disordered NbN superconductors is one prominent example [25]. Interestingly, an alternate interpretation of the data has also been put forward where the low-energy absorption has been attributed to quasiparticle effects and not to any collective modes [26]. Intermediate coupling strength demands for a nonperturbative approach, whereas the presence of disorder calls for an accurate treatment of the spatial correlations. The methods that rely on translational invariance of the Hamiltonian are not best suited to study the effect of disorder on superconductivity. Therefore, the importance of an explicit real-space approach for the study of disordered interacting fermionic systems has been realized in recent years [9,10,27].

In this paper, we present a conceptually simple and numerically efficient method for a quantitative description of the finite-temperature behavior of the AHM. The method treats the weak- and the strong-U regimes on equal footing, and captures the physics of BCS to BEC crossover. We make use of the well-known analogy of the superconducting pairing amplitudes (complex numbers) with XY spins. The parameters of the effective model are calculated by analyzing the variations in energy about the mean-field ground state by considering the relevant phase or amplitude fluctuations. A comparison of T_c estimates with other methods is presented. A quantitative description of the amplitude and phase fluctuations allows us to determine their relative importance across the BCS to BEC crossover. On the basis of the superconducting order parameter, the quasiparticle density of states, and auxiliary field distributions, we describe the metallic, superconducting, insulating, and pseudogapped phases. We find that the pseudogap phase appears close to the insulating phase, consistent with recent experiments on NbN superconductors. Finally, we demonstrate that the method works for the disordered Hamiltonian, and we discuss the possible extension to superconductors with nontrivial order-parameter symmetries.

The remainder of the paper is organized as follows. In Sec. II we discuss the model and motivation of the method. In Sec. III we present a detailed justification for the choice of the effective

classical Hamiltonian, and present schemes for obtaining the parameters of the effective Hamiltonian. The results of the model in the absence of disorder are presented and discussed in Sec. IV. In Sec. V we demonstrate the applicability of the method for disordered Hamiltonians, and the conclusions are presented in Sec. VI.

II. MODEL AND METHOD

We consider an AHM on a two-dimensional (2D) square lattice, given by

$$H = -t \sum_{\langle ij\rangle,\sigma} [c^{\dagger}_{i\sigma} c_{j\sigma} + \text{H.c.}] - U \sum_{i} n_{i\uparrow} n_{i\downarrow} - \mu \sum_{i} n_i, \tag{1}$$

where $c^{\dagger}_{i\sigma}$ and $c_{i\sigma}$ are the fermionic creation and annihilation operators. The interaction between fermions is considered attractive, as specified by the negative sign in front of the U term in the Hamiltonian. The hopping parameter t defines the basic energy scale in the model, and therefore we set $t = 1$. μ is the chemical potential which controls the average electron density in the system. For all the results presented in this paper we adjust μ so as to obtain an average filling of $\langle n\rangle = 0.8 \pm 0.01$ electrons per site.

For a mean-field treatment of this Hamiltonian, one proceeds by decoupling the interaction term in the pairing channel leading to the well-known Bogoliubov-deGennes (BdG) Hamiltonian:

$$H_{\text{BdG}} = -t \sum_{\langle ij\rangle,\sigma} [c^{\dagger}_{i\sigma} c_{j\sigma} + \text{H.c.}] - \mu \sum_{i} n_i - U \sum_{i} [\Delta_i c^{\dagger}_{i\uparrow} c^{\dagger}_{i\downarrow} + \text{H.c.}], \tag{2}$$

where $\Delta_i = \langle c_{i\downarrow} c_{i\uparrow}\rangle$ denote the local pairing amplitudes, which are complex numbers. The mean-field solution corresponds to the self-consistent values for the local variables Δ_i. Note that we do not absorb U in the definition of Δ_i. In the absence of impurities one can proceed by assuming a homogeneous solution for Δ_i, and the model can then be solved analytically by making use of the Bogoliubov transformations. In general, one proceeds by numerically diagonalizing H_{BdG} and solving for $\{\Delta_i\}$ self-consistently, without any *a priori* restrictions on them. For a given set $\{\Delta_i\}$ of auxiliary variables, H_{BdG} is diagonalized by the transformations

$$\begin{aligned} c_{i\uparrow} &= \sum_{k} (u_{k,i} \gamma_{k\uparrow} - v^{*}_{k,i} \gamma^{\dagger}_{k\downarrow}), \\ c_{i\downarrow} &= \sum_{k} (u_{k,i} \gamma_{k\downarrow} + v_{k,i} \gamma^{\dagger}_{k\uparrow}). \end{aligned} \tag{3}$$

In the above, $\gamma^{\dagger}$ (γ) are the creation (annihilation) operators for Bogoliubov quasiparticles, and the coefficients $u_{k,i}$ and $v_{k,i}$, which satisfy $\sum_k |u_{k,i}|^2 + |v_{k,i}|^2 = 1$ for each site i, are obtained numerically [28].

The BdG mean-field method correctly captures the BCS solution in the weak-coupling limit, and describes the transition temperature and the superconducting gap accurately. However, in the strong-U limit it severely overestimates the superconducting transition temperature (T_c). It is well known that in the strong-coupling limit the superconducting order at low temperature can be understood as a BEC of preformed cooper pairs. Therefore, an effective phase-only model is commonly used to describe the strong-coupling limit [29]. In order to capture the weak to strong-coupling crossover, one needs to go beyond the BdG mean-field scheme.

Quantum Monte Carlo (QMC), which is sign-problem free for the AHM, clearly provides a very accurate way to study the model at arbitrary coupling strength. However, the method is computationally intensive. In the determinantal QMC algorithm using the Suzuki-Trotter decomposition, for example, the simulation scales as $N^3 L$, where N is the size of the spatial lattice and L is the size of the lattice in the (Matsubara) time direction. Typical lattice sizes that can be studied using QMC are 18×18 sites [30]. Therefore, it becomes difficult to analyze effects of disorder on superconductivity using QMC. Another approach that has been proposed for studying models of superconductivity with quenched disorder is the static-auxiliary-field Monte Carlo (SAF-MC) [27]. This is a static version of the QMC where the temporal dependence of the auxiliary fields is ignored, and only the spatial dependence is retained. This method reduces to the BdG mean-field method at $T = 0$; however, it captures the fluctuations in both amplitude and phase of the superconducting order parameters Δ_i and therefore captures the finite-temperature physics of a superconductor at arbitrary interaction strengths. The computational time for this method scales as N^4, and therefore one is still severely limited in terms of accessible lattice sizes. Therefore, further approximations are commonly used to achieve larger sizes [31–33].

Here, we propose that an effective classical Hamiltonian H_{cl} can be used to generate configuration for the complex auxiliary field Δ_i. These configurations can be generated numerically using the standard importance sampling with the Metropolis algorithm. Our proposed classical Hamiltonian is given by

$$\begin{aligned} H_{\text{cl}} &= H_{\text{phase}} + H_{\text{amp}}, \\ H_{\text{phase}} &= -\sum_{ij} J_{ij}(T) \cos(\phi_i - \phi_j), \\ H_{\text{amp}} &= \sum_{i} k_i(T) [|\Delta_i| - \Delta_0(T)]^2. \end{aligned} \tag{4}$$

In the above, ϕ_i and ϕ_j denote the phases of the superconducting amplitudes Δ_i and Δ_j at sites i and j, respectively. The temperature-dependent parameter $J_{ij}(T)$ denotes the phase stiffness, which will also be bond dependent in the disordered case. The term H_{amp} captures the effect of amplitude fluctuations about the mean amplitude value, $\Delta_0(T)$, for a given temperature. The amplitude stiffness parameter, $k_i(T)$, is in general dependent on site as well as temperature. For the clean case the phase and amplitude stiffness parameters are spatially uniform. We further assume that both these parameters are also independent of temperature. However, it is very important to retain the temperature dependence of the $\Delta_0(T)$ as will be discussed later. Within a semiclassical approach, the physics of the Hamiltonian Eq. (1) can then be described by a combination of H_{cl} and H_{BdG}. The H_{BdG} describes the response of the fermions to a configuration of classical auxiliary field Δ_i, and

the evolution of the auxiliary field is approximately captured by the classical Hamiltonian $H_{\rm cl}$. This approach is similar, in spirit, to the methods proposed for describing magnetism in the double-exchange model [34,35]. The simulations begin at low temperature and we assume the starting state to be a phase coherent superconducting state. The mean-field solution is obtained at each temperature. By analyzing the nature of fluctuations around the mean-field solution, as will be discussed in the next section, we define the parameters for the $H_{\rm cl}$. The resulting $H_{\rm cl}$ is then simulated via Monte Carlo, and electronic properties are obtained by using the configurations for Δ_i into $H_{\rm BdG}$. The Metropolis algorithm with the standard single-site updates is employed for simulations. Most of the results presented here are obtained on a square lattice with $N = 40^2$ sites. The number of Monte Carlo steps used for equilibration and averaging of quantities involving classical auxiliary variables is $\sim 10^5$. Since electronic properties require a solution of Schrödinger equation for each configuration, thermal averaging for electronic properties is performed over $\sim 10^3$ Monte Carlo steps.

III. PARAMETERS OF THE EFFECTIVE HAMILTONIAN

We begin by analyzing the nature of fluctuations about the BdG mean-field solution of the AHM. Given the complex nature of the variables $\Delta_i \equiv |\Delta_i| e^{i\phi_i}$ we can compute the change in energy caused by the variation in the phases ϕ_i and that caused by the change in amplitudes $|\Delta_i|$. In order to provide a simple geometrical picture, the Δ_i can be viewed as 2D rotors of variable length $|\Delta_i|$.

It is well known that in the strong-coupling limit the XY model captures the physics of phase fluctuations. Moreover, the simplest scalar that can be constructed from two vectors is their dot product. Therefore, it is reasonable to assume that the change in energy due to relative change of orientation between pairs of rotors is described by the first term in $H_{\rm cl}$ Eq. (4), i.e.,

$$H_{\rm phase} = -\sum_{ij} J_{ij} \cos(\phi_i - \phi_j),$$

where, in principle, all pairs ij can contribute to the summation. The task is now to determine the coupling constants J_{ij}, which in a translationally invariant system should only depend on the distance between sites i and j. Suppose E_0 is the energy of the self-consistent BdG solution that in the rotor picture corresponds to all rotors pointing in the same direction, say $\phi_i \equiv 0$. Now we change the orientation of the rotor at the ith site by an angle θ so that $\phi_i = \theta$, and compute the change in energy δE_1. Within the effective rotor model, $H_{\rm phase}$, this change must be attributed to the change in bonds that connect the ith site to all other sites [see Fig. 1(a)]. Next, we restore the orientation of the ith rotor back to $\phi_i = 0$, and change the orientation of the rotor at the jth site by the same angle θ [see Fig. 1(b)]. This leads to a change in energy δE_2 which is coming from the change in bonds that are connecting the jth site to all other sites. Clearly, for a translationally invariant system we should have $\delta E_2 = \delta E_1$. Then we orient both the ith and the jth rotors at an angle θ, i.e., $\phi_i = \phi_j = \theta$. The change is energy obtained in this configuration is δE_3. The change in this case is coming from the change in all the bonds connecting ith and jth rotors to all other rotors, except to each other [see Fig. 1(c)]. Therefore, we can identify the coupling strength between the ith and the jth rotors as $2J_{ij} = \delta E/(1-\cos\theta)$ where $\delta E = (\delta E_1 + \delta E_2 - \delta E_3)$. Using this protocol for calculating the coupling constants, we can also compute the longer-range coupling strengths. Note that we are not assuming that only nn bonds contribute to the summation in Eq. (4). In fact, the present scheme for calculating the J_{ij} shows explicitly that the most important coupling is that between the nearest

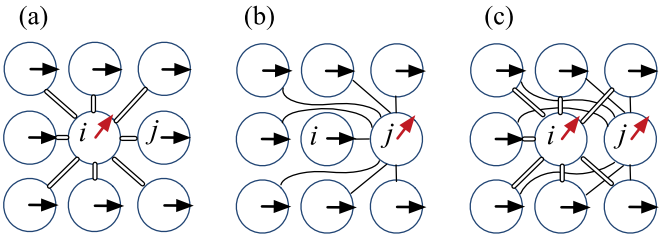

FIG. 1. A schematic picture describing the method to isolate the contribution of a single rotor pair to the total energy for the effective classical Hamiltonian. (a) i th rotor is oriented away from the otherwise phase coherent arrangement of rotors. The double lines connecting site i to all other sites indicate the pairs that contribute to the change in energy due to change in the orientation of the i th rotor. (b) j th rotor is rotated by an angle θ, and the single lines indicate the pairs contributing to change in energy. (c) Both i th and j th rotors are rotated by an angle θ. Note that in this case the pair ij does not contribute to the change in energy.

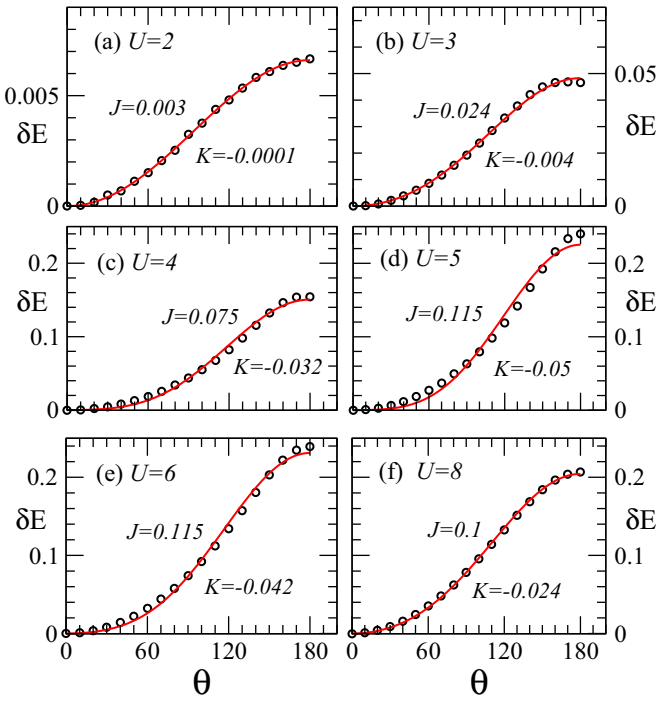

FIG. 2. (a)–(f) Change in energy as a function of the orientation angle between a single nearest-neighbor pair of rotors for different values of U. Symbols are the results of numerical calculations and the solid line in each panel is a fit to the functional form $J(1-\cos\theta) + K(1-\cos^2\theta)$. The best-fit values of J and K are indicated in the figure.

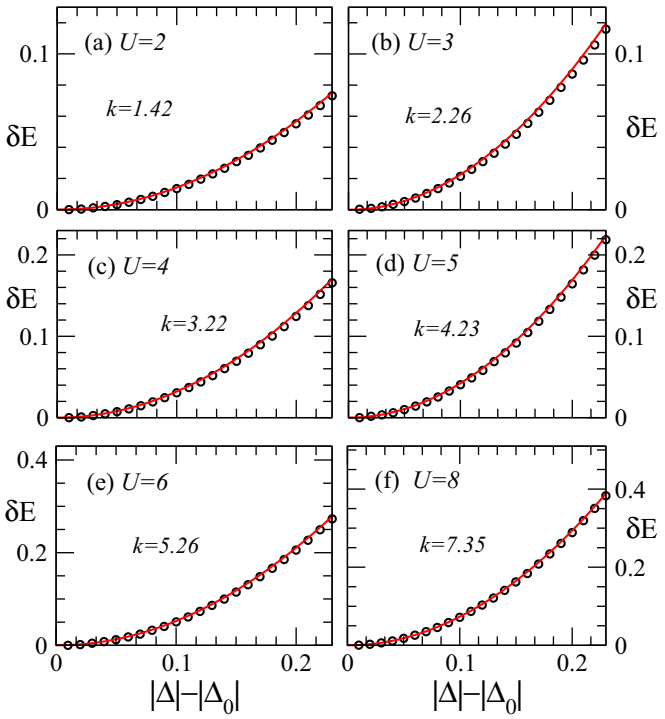

FIG. 3. (a)–(f) Change in energy as a function of the change in magnitude of a single rotor. Symbols are the numerical data and the solid line shows a fit to the functional form $\delta E = k(|\Delta| - |\Delta_0|)^2$, with the values of best-fit parameter noted in the figure.

neighbor i,j pairs. Moreover, the protocol proposed above for computing coupling strengths also works for a disordered system, where J_{ij} will now depend on the sites i and j, and therefore we will get a distribution of coupling strengths even for nearest-neighbor couplings.

We begin by verifying the validity of the $\cos(\phi_i - \phi_j)$ form that is assumed in the effective classical Hamiltonian. Figure 2 shows the numerical data for change in energy δE as a function of angle of orientation θ for different values of attractive Hubbard parameter U. The function $f(\theta) = J(1 - \cos\theta) + K(1 - \cos^2\theta)$ fits the numerical data very well for all values of U. The best-fit parameter J is much larger than K, therefore in the simplest approximation we retain only the $\cos(\phi_i - \phi_j)$ form in the effective Hamiltonian Eq. (4). In order to compute the values of the coupling parameters J_{ij} one can use either the best-fit values, as indicated in Fig. 2, or any two points from the numerical data.

Following an analogous approach we justify the use of the second term in the effective Hamiltonian. This term can be written as $H_{\rm amp} = \sum_i k_i(|\Delta_i| - |\Delta_0|)^2$, and represents the stiffness to the change in magnitude of the local pairing amplitude compared to the average magnitude in the self-consistent solution. Given the on-site nature of this term, it is easier to compute the change in energy. The results are shown in Fig. 3, which shows the change in energy due to the change in the length of the rotor for different U. In this case the function $g(\delta|\Delta|) = k(\delta|\Delta|)^2 \equiv k(|\Delta| - |\Delta_0|)^2$ fits the numerical data very well, hence justifying the form of the second term in the effective Hamiltonian. The rotor picture for the superconducting amplitudes is strictly valid in the large-U limit. This is analogous to how in the repulsive Hubbard model a local magnetic moment is well defined only in the large-U limit. Therefore, an alternate approach is used to find the phase stiffness constant in the small-U regime. This is obtained from the the expectation value of the kinetic-energy operator [36].

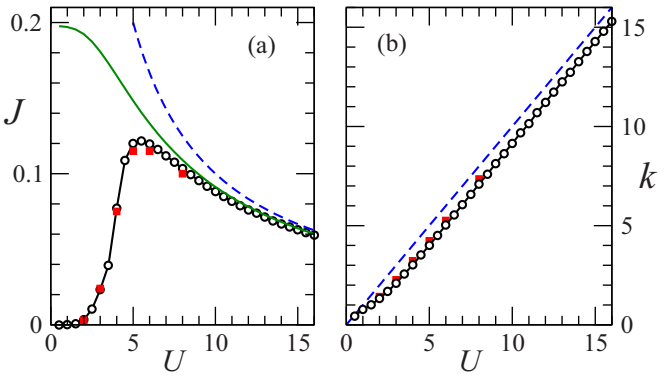

FIG. 4. Parameters of $H_{\rm cl}$ as extracted from the change in energy about the mean-field value. (a) Coupling constant J (open circles) as a function of U calculated by assuming a cosine form for the change in energy and using only $\theta = 0$ and π. Filled squares show a comparison with J obtained from the fits shown in Fig. 2. Green solid line is the phase stiffness calculated as expectation value of the kinetic-energy operator. The dashed blue line represents the $1/U$ behavior valid in the large-U limit. (b) The stiffness k to change in local amplitude $|\Delta_i|$, as a function of U calculated by assuming a $k(|\Delta| - |\Delta_0|)^2$ form and using only two points from the data (open circles). Filled squares are the values obtained from the best fits shown in Fig. 2. Dashed blue line represents $k = U$.

In the following, we summarize the behavior of the parameters of our $H_{\rm cl}$. Figure 4(a) shows the plot of nn coupling constant J as a function of U. The values obtained via the best fit to the cosine form [filled squares in Fig. 4(a)] and those obtained by using only $\theta = 0,\pi$ on the cosine curve (open symbols) match very well. In the large-U limit, we find that $J \sim t^2/U$ as expected from the strong-coupling expansion [dashed line in Fig. 4(a)].

For $U \leqslant 5$, J decreases upon decreasing U. This indicates a breakdown of the local description for the superconducting amplitudes as the phase stiffness at weak coupling should not go to zero in a superconducting phase. In the low-U regime, we need to choose an alternate approach for computing the phase stiffness parameter J. Within the Kubo linear-response formalism, the superfluid stiffness consists of diamagnetic and paramagnetic parts [37]. The diamagnetic part is related to the expectation value of kinetic energy per link [28,36,37]. Following Ghosal *et al.* [28] the kinetic energy can be computed as

$$-E_{\rm kin} = 4t/N \sum_{i,k} v_{k,i}\, v_{k,i+\hat{x}}, \tag{5}$$

where $v_{k,i}$, etc., are the coefficients appearing in the Bogoliubov transformations Eq. (3). At low temperatures, the paramagnetic contribution to the superfluid stiffness is negligible [36]. Therefore, the kinetic energy per link is a measure of the phase stiffness parameter J for the entire range of U values. This serves as a cross-check for our calculation of J_{ij}

described above. The variation of $-E_{\rm kin}$ with U is shown as a solid line in Fig. 4(a). Indeed, for values of U larger than ∼5 the kinetic energy per link matches well with the J computed in terms of energy cost for relative phase change. Therefore, in the disorder-free case we use $-E_{\rm kin}$ as the phase stiffness parameter J for the entire range of U.

The amplitude stiffness parameter k as a function of U is shown in Fig. 4(b). Once again using a best fit to the quadratic form (filled squares) and using only two points from the numerical data (open symbols) are very close. The dashed line corresponds to $k = U$, and seems to be a good approximation for the stiffness constant over the entire U range.

IV. MONTE CARLO SIMULATION RESULTS

A. Order parameter and auxiliary variable distributions

We define the superconducting order parameter at finite temperature by $\Delta_{\rm op} = \frac{1}{N}\langle\sum_i \Delta_i\rangle$, where the angular brackets denote thermal averaging over Monte Carlo configurations of auxiliary variables and N is the number of sites. The temperature dependence of $\Delta_{\rm op}$ for different values of U is shown in Fig. 5(a). The point of inflection in $\Delta_{\rm op}(T)$ is used to estimate the value of the superconducting transition temperature T_c. The transition temperature displays a nonmonotonic behavior with varying U [see Fig. 5(a)]. The sharp reduction in $\Delta_{\rm op}$ across T_c is caused by the vanishing of $|\Delta_i|$ for small U, and by randomness in phases ϕ_i for large U. These two limits are connected smoothly with variation in U, as will be discussed in detail in the following.

In order to compare with the state-of-the-art QMC results, for example those presented in Ref. [30], we compute the pair-pair correlation function, P_S, defined as

$$P_S = \frac{1}{N}\sum_{ij}\langle c^\dagger_{i\uparrow}c^\dagger_{i\downarrow}c_{j\downarrow}c_{j\uparrow} + \text{H.c.}\rangle. \qquad (6)$$

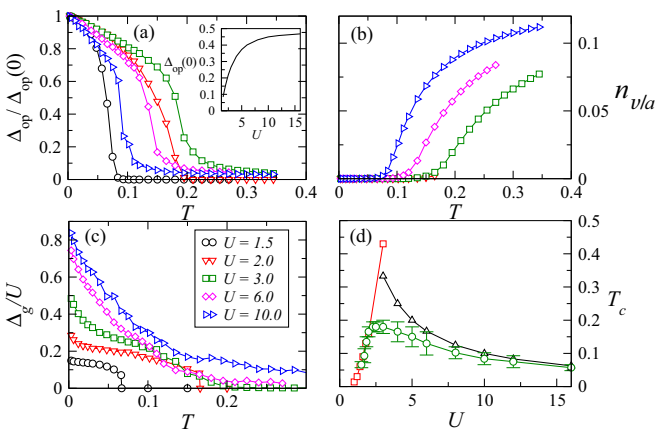

FIG. 5. (a) The temperature dependence of the superconducting order parameter $\Delta_{\rm op}$ normalized by its low-temperature value, $\Delta_{\rm op}(0)$, for different values of U. Inset shows the variation of $\Delta_{\rm op}(0)$ with U. (b) Vortex n_v and antivortex n_a density as function of temperature. (c) Spectral gap Δ_g as a function of temperature for different U. (d) Circles show the transition temperature T_c, as inferred from the inflection point in the T dependence of the order parameter, as a function of U. Squares and triangles mark, respectively, the expected variations of T_c in the small-U and large-U limits.

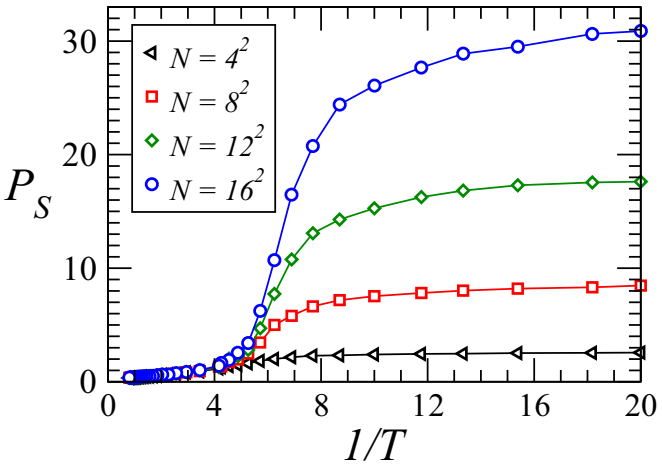

FIG. 6. Variation of the pair-pair correlation function P_S with inverse temperature for different system sizes. The results are obtained for $U = 4t$ and $n \approx 0.5$.

The results are presented in Fig. 6. The values of P_S below critical temperature are larger than those obtained in the QMC simulations [30]. This can be attributed to the absence of quantum fluctuations in the present treatment where the temporal fluctuations in the auxiliary fields are completely ignored. This is along the lines of the SAF-MC method proposed recently [27]. Two important features that are consistent with the QMC results are (i) the absence of size dependence for small values of inverse temperature and (ii) a systematic scaling with the system size for large values of β. These features are important for extracting a value of critical temperature from the computed data. Clearly, similar information is contained in the $\Delta_{\rm op}(T)$ plots shown in Fig. 5(a). A quantitative comparison of P_S with the QMC results suggests that the present method overestimates the magnitude of the order parameter in the superconducting phase. Similarly, T_c values are overestimated compared to the QMC results. It is important to point out that the present method is not capable of describing quantum phase transitions, which are solely driven by quantum fluctuations.

A useful quantity that determines the importance of the phase of the superconducting order parameter is the vorticity [38]. Vorticity (antivorticity) can be defined as the sum of difference of phases around a square plaquette taken clockwise (anticlockwise) and summed over all plaquettes. The difference in angles $\phi_j - \phi_i$ is defined modulo $\pm\pi$. The density of vortices and antivortices ($n_{v/a}$) is shown in Fig. 5(b). In the weak-coupling regime there are no vortex/antivortex excitations as the system goes across the transition [see Fig. 5(b) for $U = 1.5$ and 2]. This shows that the transition is caused solely by fluctuations in amplitudes of the local superconducting order parameters Δ_i. Indeed, for intermediate to large values of U, density of vortices begins to rise near the transition temperature as determined from $\Delta_{\rm op}$. This is consistent with previous results obtained in the extreme large-U limit, where one can assume the magnitudes $|\Delta_i|$ to be constant and the fluctuations are captured by a phase-only XY model [38].

The electronic spectrum is obtained in the Monte Carlo generated auxiliary field configurations by solving for $H_{\rm BdG}$ Eq. (2). One of the important features contained in the electronic spectra is the spectral gap, which we define as the energy difference between lowest unoccupied level and highest occupied level assuming a $T = 0$ Fermi distribution function. The spectral gap normalized to the value of U is plotted in Fig. 5(c). The temperature dependence shows that the gap vanishes at T_c for small values of U, whereas it remains finite even in the nonsuperconducting regime for intermediate to large values of U. The U dependence of T_c obtained in present study is consistent with the BCS result for small U and a strong-coupling $1/U$ behavior for large U [Fig. 5(d)]. These results are qualitatively similar to those obtained by the dynamical mean-field theory (DMFT), QMC, and other computationally demanding methods. The quantitative features are as follows. The maximum value of T_c is $0.18t$, and occurs near $U = 3.0t$. Within various methods these characteristic scales are, respectively, given by $0.12t$ and $2t$ (T-matrix approximation), $0.2t$ and $4t$ (DMFT), $0.16t$ and $4t$ (fluctuation exchange approximation), $0.18t$ and $5t$ (QMC), and $0.14t$ and $5t$ (SAF-MC) [27,39–41]. Although the maximum value of T_c and the corresponding U value should both depend on the average electron density, within QMC this dependence is insignificant in the density range $0.5 < n < 0.9$, and hence the above comparison is meaningful despite the different values on n used in different studies [30].

The introduction of an effective classical Hamiltonian for auxiliary fields has twofold advantage. First, it facilitates the application of the Monte Carlo procedure; second, the behavior of auxiliary variables provides additional insight into the nature of the finite-temperature transitions. In order to further understand the difference between the superconducting to normal state transitions at weak and strong coupling, we investigate the details of the temperature evolution of local pairing amplitudes, Δ_i. The distribution of the magnitude of pairing amplitudes is computed via

$$P(|\Delta|) = \frac{1}{N}\left\langle \sum_i \delta(|\Delta| - |\Delta_i|)\right\rangle, \tag{7}$$

where the Dirac-delta function is approximated by a Lorentzian with width $\eta = 0.01$. The resulting distribution is plotted in Figs. 7(a)–7(c). At low T the mean value of the distribution increases with increasing U. The width of the distribution decreases with increasing temperature for $U = 1.5$ due to a decrease in Δ_0 with increasing T [see Fig. 7(a)]. At large U, since Δ_0 becomes almost independent of T, an expected increase in the width of the distribution due to thermal effects is obtained in our simulations [see Fig. 7(c)]. Interestingly, a combination of these two effects occurs at intermediate U where the width first increases and then decreases upon increasing T [see Fig. 7(b)]. In order to assess the relative importance of the amplitude fluctuations in driving the system to a normal state, we compute the ratio of the variance to the mean value of the distribution. This is plotted as a function of U for $T \sim T_c$ in Fig. 7(d). Clearly, the amplitude fluctuations become less important upon increasing the strength of attractive coupling. Nevertheless, such fluctuations are always present, and seem to vanish only asymptotically.

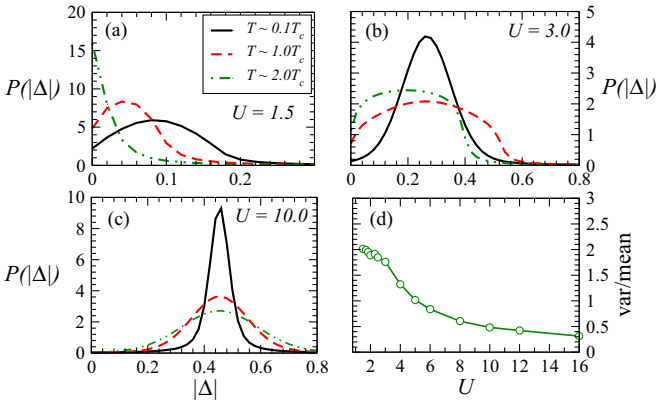

FIG. 7. The distribution $P(|\Delta|)$ of magnitudes $|\Delta|$ at different temperatures, $0.1T_c$, $1.0T_c$, $2.0T_c$, for (a) $U = 1.5$, (b) $U = 3$, and (c) $U = 10$. (d) The ratio of the variance to the mean value of $P(|\Delta|)$ as function of U. This ratio decreases with increasing U highlighting the importance of amplitude fluctuations at weak U values.

Next, we discuss the fluctuations in the phase of the superconductor along the same lines as those in amplitudes. We define a bond variable $D_{ij} = \cos(\phi_i - \phi_j)$, where i and j are the nn sites, and compute the distribution of D_{ij} as

$$P(D) = \frac{1}{N}\left\langle \sum_{\langle ij\rangle} \delta(D - D_{ij})\right\rangle. \tag{8}$$

The δ function is approximated by a Lorentzian as before. The distributions are shown in Figs. 8(a)–8(c) for different values of U and T. For all values of U, the distribution is sharply peaked near $D = 1$ at low temperatures, and becomes progressively broader with increasing temperature. The inverse of peak height of the distribution can be taken as an indicator for the width of the distribution. In Fig. 8(d) we show the peak height as a function of T for three values of U. For intermediate and large U, the peak height reduces strongly with temperature, indicating stronger fluctuations

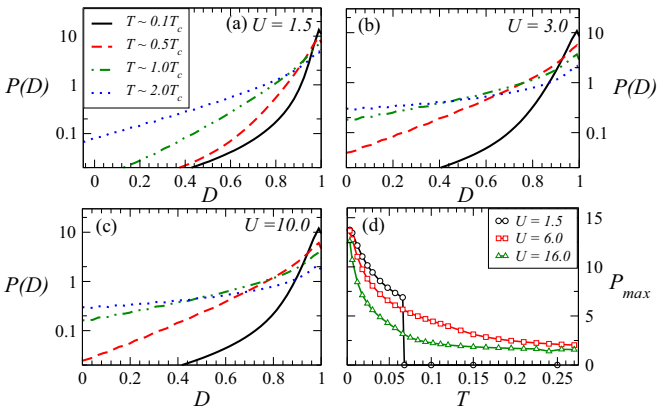

FIG. 8. The distribution $P(D)$ of the nn phase correlators $\cos(\phi_i - \phi_j)$ (see text) at different temperatures, $0.1T_c$, $0.5T_c$, $1.0T_c$, $2.0T_c$, for (a) $U = 1.5$, (b) $U = 3$, and (c) $U = 10$. (d) The maximum value, $P_{\rm max}$, of $P(D)$ as a function of T for various U values.

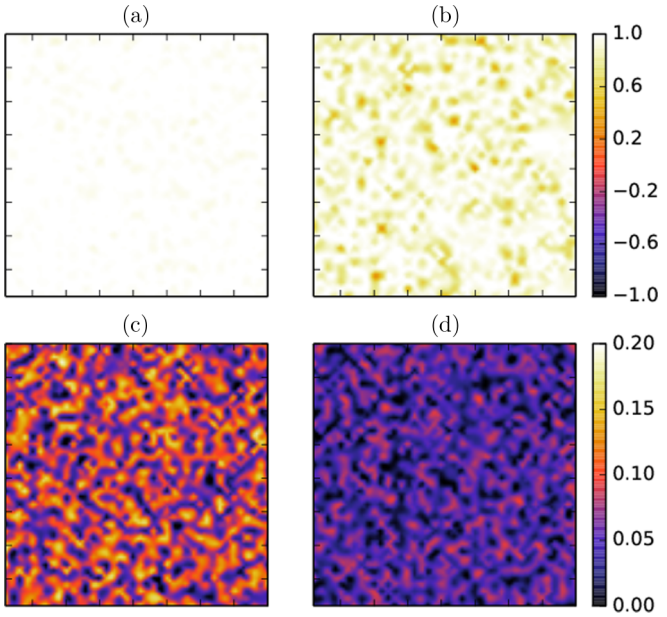

FIG. 9. Real-space plots for two different temperatures $T \sim 0.1T_c$ (first column) and $T \sim T_c$ (second column) for $U/t = 1.5$. (a) and (b) show the nn phase correlations $D_{ij} = \cos(\phi_i - \phi_j)$, and (c) and (d) show the amplitude variables $|\Delta_i|$.

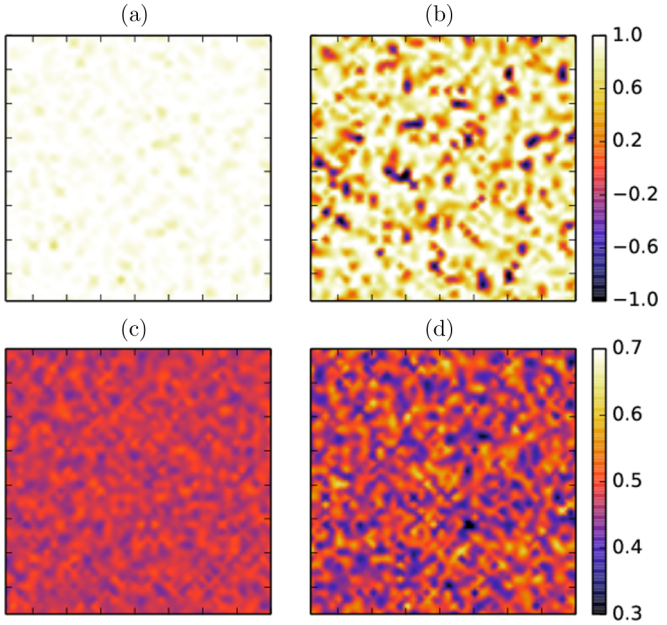

FIG. 10. Real-space plots for two different temperatures $T \sim 0.1T_c$ (first column) and $T \sim T_c$ (second column) for $U/t = 16$. (a) and (b) show the nn phase correlations $D_{ij} = \cos(\phi_i - \phi_j)$, and (c) and (d) show the amplitude variables $|\Delta_i|$.

in the phase. The results are, therefore, consistent with the well-known notion that for strong interactions the phase fluctuations are dominant. The overall behavior of amplitude and phase fluctuations shows that for a wide intermediate range of U both the amplitude and phase fluctuations play important roles in driving the superconducting state towards a normal state.

We plot the configurations of the auxiliary variables in terms of the amplitude and the phase of Δ_i. The plot is shown in Fig. 9 for $U = 1.5$ and in Fig. 10 for $U = 16$ at $T \sim 0.1T_c$ and T_c. For small U the fluctuations in the phase $\{\phi_i\}$ are essentially absent at $T \sim 0.1T_c$, and remain insignificant even as T approaches T_c [see Figs. 9(a) and 9(b)]. On the other hand, the amplitudes $\{|\Delta_i|\}$ show significant fluctuations already at $T \sim 0.1T_c$, which become very strong as T approaches T_c [see Figs. 9(c) and 9(d)]. This reconfirms that the small-U regime is dominated by amplitude fluctuations. The trends are essentially reversed for large U. The phase fluctuations are relatively stronger for $U = 16$ [see Figs. 10(a) and 10(b)]. The amplitudes also contain significant fluctuations, but remain finite even at T_c [see Figs. 10(c) and 10(d)]. Therefore the loss of superconductivity in the large-U limit is driven by the fluctuations in the phase. While the dominant fluctuations can be identified as amplitudelike for weak U and phaselike for strong U, fluctuations in both the phase and amplitude variables are present over the full range of the attraction strength. The idealized amplitude-only and phase-only descriptions of the suppression of superconducting order seem to be valid only in very small-U and very large-U regimes of the model. This is supported by experiments where presence of Josephson effect, which is an indicator for phase-sensitive superconductivity, is observed over the entire BCS to BEC crossover region [16].

B. Quasiparticle DOS and pseudogap phase

The behavior of the classical auxiliary variables with increasing temperature and for different U already provides us with substantial insight into the thermal physics of the superconductor. It is equally important to analyze the response of the quasiparticles to the thermal fluctuations at different values of U. To this end, we now discuss the behavior of the quasiparticle density of states, which is defined as

$$N(\omega) = \frac{1}{N}\left\langle \sum_k \delta(\omega - \epsilon_k) \right\rangle, \tag{9}$$

where ϵ_k are the $2N$ eigenvalues obtained numerically by solving for H_{BdG} Eq. (2) in a given configuration of the classical auxiliary variables. The angular bracket denotes averaging over various Δ_i configurations as generated by the Monte Carlo. The DOS across the entire range of T and U can be grouped into three qualitatively distinct categories based on their behavior near the chemical potential. These are (i) gapped, (ii) pseudogapped, and (ii) gapless (see Fig. 11). At $T = 0$ the DOS supports a finite spectral gap for all values of U. However, the finite T behavior depends strongly on the value of U. For small U, the gap vanishes as $T \geqslant T_c$ [see Fig. 11(a)]. For very large U the gap persists above T_c [see Figs. 11(c) and 11(d)]. In the intermediate- to strong-U regime, the DOS shows a dip at chemical potential without a clean gap. This regime of parameter space is termed as a pseudogap regime.

In order to find a possible connection between the nature of the DOS as discussed above and the nature of fluctuations in the auxiliary field variables we consider the following three idealized configurations of auxiliary variables. These are (i) amplitude-only fluctuations—configurations with perfect

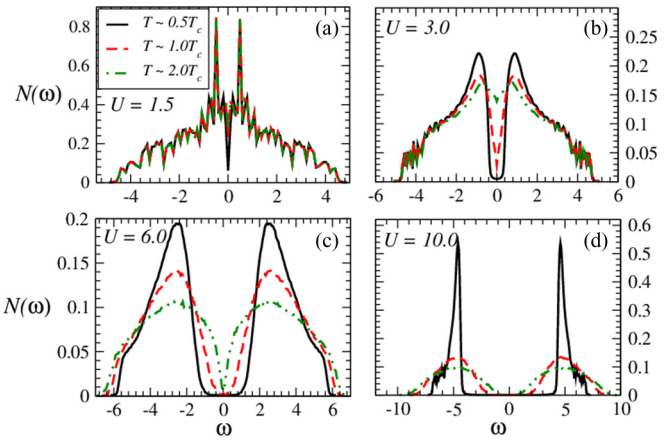

FIG. 11. Variation of quasiparticle density of states, $N(\omega)$, with temperatures for coupling strengths (a) $U = 1.5$, (b) $U = 3$, (c) $U = 6$, and (d) $U = 10$. For small U, the spectral gap vanishes at T_c as expected in the BCS regime.

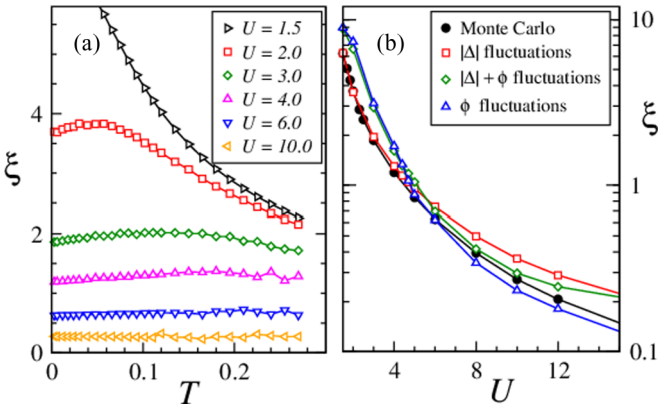

FIG. 12. (a) Temperature variation of coherence length (ξ) for different U. (b) Variation of ξ as function of U at low temperatures. The filled symbols represent the Monte Carlo data, and the other three data sets are for the hypothetical auxiliary field configurations corresponding to fluctuations in magnitude of Δ_i, phase of Δ_i, and both phase and magnitude of Δ_i (see text).

phase coherence ($\phi_i \equiv \phi_0$), but a random distribution of $|\Delta_i|$ between zero and $2|\Delta_0|$, where Δ_0 is the low-temperature value of the order parameter—(ii) phase-only fluctuations—the amplitudes are uniform ($|\Delta_i| \equiv |\Delta_0|$) and the phases are randomly distributed between zero and 2π—and (iii) amplitude and phase fluctuations—both $|\Delta_i|$ and ϕ_i are randomly distributed over the above-mentioned range. The DOS is computed for these three idealized configurations for different values of U. The outcome of this in terms of the nature of DOS is presented in Table I. We find that amplitude-only fluctuations do not lead to a pseudogapped DOS. For the other two combinations, the pseudogap phase occurs for intermediate values of U, and a fully gapped DOS above T_c is consistent with both phase-only and amplitude and phase fluctuations. Within the analysis presented in Table I, a pseudogap phase exists at intermediate values of U when phase fluctuations are present. However, the auxiliary field distributions generated during Monte Carlo are such that the phase fluctuations at intermediate U are necessarily accompanied by amplitude fluctuations. Therefore, one can conclude that a pseudogap phase exists when both phase and amplitude fluctuations are present. Recent experiments indeed show that a pseudogap phase can exist in conventional superconductors that sit at the proximity to an insulating phase [42].

TABLE I. Nature of DOS at $T > T_c$ for different values of U within three basic scenarios that consider different combinations of fluctuations in magnitude and phase of Δ_i.

U ⇓, Fluctuations ⇒	$\{\lvert\Delta_i\rvert\}$	$\{\lvert\Delta_i\rvert\} + \{\phi_i\}$	$\{\phi_i\}$
1.5	Gapless	Gapless	Gapless
2.0	Gapless	Gapless	Gapless
3.0	Gapped	Pseudogapped	Pseudogapped
4.0	Gapped	Pseudogapped	Pseudogapped
6.0	Gapped	Gapped	Gapped
8.0	Gapped	Gapped	Gapped
16.0	Gapped	Gapped	Gapped

Another indicator that is commonly used to describe the crossover from a BCS-like superconductor to the BEC of cooper pairs is the coherence length of the superconductor. The coherence length ξ is defined via [11]

$$\xi^2 = \frac{\sum_r r^2 |F(r)|^2}{\sum_r |F(r)|^2}, \tag{10}$$

where $F(r) = \frac{1}{\sqrt{N}} \sum_i \langle c_{i+r\downarrow} c_{i\uparrow} \rangle$, and $i + r$ denotes a site located at distance r from site i. Figure 12(a) shows the temperature dependence of pair coherence length for different values of U. For small values of U, the coherence length decreases with temperature, and $\xi(T_c)/\xi(0) \sim 0.8$ in agreement with previous calculations [11]. With increasing U, ξ reduces rapidly and becomes essentially temperature independent. Note that $\xi < 1$ for $U > 4$ indicates that the cooper pairs have essentially become well localized in this regime of interaction strength. We further test the three basic scenarios of fluctuations in auxiliary variables for the pair coherence length. We compare the results obtained for the pair coherence length in the Monte Carlo simulations, with those obtained by considering three types of idealized auxiliary variable configurations that are already discussed for the DOS. We find that for small values of U our Monte Carlo simulation results for ξ are very close to those obtained in the amplitude-only fluctuation model [see Fig. 12(b)]. In the large-U regime, the Monte Carlo results are closest to the phase-only fluctuation model. In the intermediate range, $4 < U < 10$, the coherence length is best described by the fluctuations in both $|\Delta_i|$ and ϕ_i These results indicate that the Monte Carlo method faithfully captures the crossover from amplitude-only fluctuation regime at small U to the XY-model regime at large U.

We summarize the results obtained so far in a phase diagram in Fig. 13(a). The T-U phase diagram as obtained within our simulations consists of four distinct phases, namely, SC, normal metal, non-SC gapped, and pseudogapped. This is consistent with results obtained via more sophisticated numerical techniques. The pseudogapped state can be understood as an indicator for the presence of both the phase and the amplitude

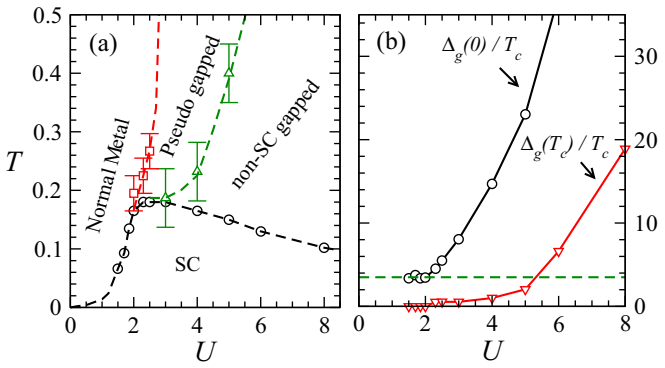

FIG. 13. (a) The T-U phase diagram showing the superconducting, the normal metal, the nonsuperconducting gapped, and the pseudogapped phases. Symbols are the data points obtained from simulations and the dashed lines are guides to eye. (b) The ratio of spectral gap to ordering temperature, $\frac{\Delta_g}{T_c}$, as a function of U. The ratio is shown for the gap at $T = 0$ and that at $T \sim T_c$.

fluctuations. The turnaround of the T_c versus U curve, which is located close to the BCS behavior within our calculations, can be considered as an indicator for the onset of significant phase fluctuations. This is why the region just above T_c shows pseudogapped DOS. As U increases, the phase fluctuations become dominant, however the amplitude fluctuations become inactive only when U is considerably large. The DOS remains gapped as long as amplitude fluctuations are weak, and at higher T when both amplitude and phase are random, a pseudogap phase appears. The pseudogap phase is likely to disappear at a scale proportional to U itself, where the pairing amplitudes themselves vanish and therefore the phase of the order parameter cannot be defined. In Fig. 13(b) we show the plot of $\Delta_g(0)/T_c$ as a function of U. The plot begins to deviate from the BCS value of 3.5 (as indicated by the horizontal dashed line) around $U = 2$. We also show $\Delta_g(T_c)/T_c$ as a function of U. In the BCS scenario, $\Delta_g(T_c)/T_c = 0$, which we find to hold for $U \leqslant 3$. These two indicators of BCS behavior suggest that the deviation from a BCS-like superconducting order begins somewhere between $U = 2$ and 3. However, there is no critical value of U for which the behavior deviates from the BCS behavior.

V. EFFECTIVE HAMILTONIAN IN THE PRESENCE OF QUENCHED DISORDER

Although disorder is present to varying degrees in almost all materials, its effect is typically ignored in the simplest treatment. Indeed, translational invariance is commonly invoked in theories of condensed-matter systems. In the context of superconductors, however, disorder plays a crucial role in providing a better understanding of the underlying mechanisms. Indeed, there has been immense interest in studying disordered superconductors, both bulk and thin films, in recent years [25,42]. The idea is to use disorder as a control parameter which then provides new insights into the understanding of correlated electron physics. Hence, methods that can treat the effect of disorder accurately become extremely useful. This is where the real-space methods hold an edge over the variety of mean-field methods. Having shown that the real-space method proposed in Sec. II of this paper recovers the physics of thermal fluctuations in both the amplitude and the phase of the superconducting order, we now demonstrate that the scheme can be applied to disordered Hamiltonians. In order to proceed, we use the prototype model for disorder and extend our Hamiltonian Eq. (1) by adding a random on-site energy term. The resulting disordered Hamiltonian is given by

$$H' = H + \sum_i \epsilon_i (n_{i\uparrow} + n_{i\downarrow}), \tag{11}$$

where ϵ_i are random variables selected from a uniform box distribution of width V, i.e., $-V < \epsilon_i < V$. The additional term affects both $H_{\rm BdG}$ Eq. (2) and $H_{\rm cl}$ Eq. (4). The change in $H_{\rm BdG}$ is simply the addition of the term $\sum_i \epsilon_i n_i$ to Eq. (2). The change in $H_{\rm cl}$ arises via the change in the parameters of the effective Hamiltonian. Since translational symmetry is broken by the disorder term, the parameters J_{ij} and k_i in Eq. (4) become site dependent. However, even before arriving at the effective parameters, we need to verify the validity of the form of the effective Hamiltonian Eq (4). We show the dependence of the change in energy on the rotation angle for all nn pairs of sites. Since our primary task is to identify the functional form of $\delta E(\theta)$, we plot the change in energies normalized to the change for largest value of θ, i.e., $\theta = \pi$ for all nn pairs. The resulting plot is shown in Fig. 14 for a few representative values of U and V. While there is a broadening due to disorder, the overall shape of the curve is reasonably well

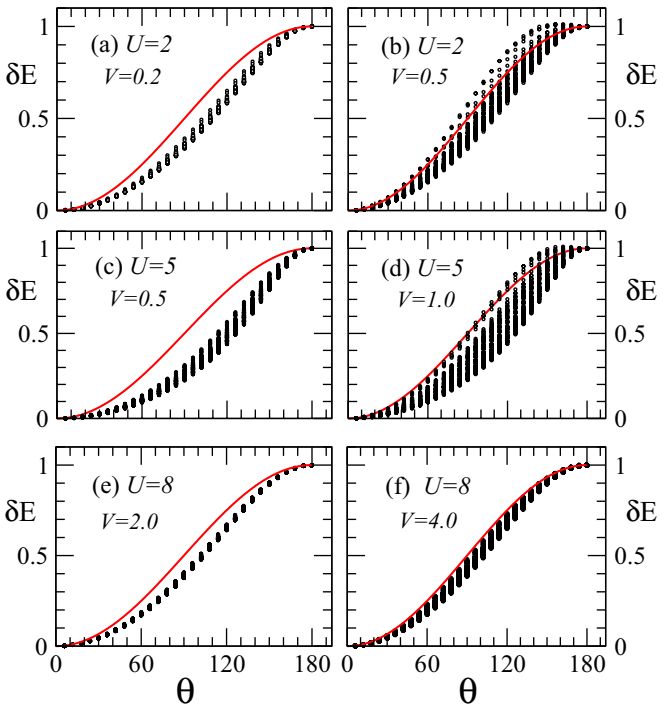

FIG. 14. (a)–(f) Change in energy as a function of the orientation angle between a single pair of rotors for different values of U and V. The scatter of points is due to the inequivalence of nearest-neighbor pairs. In order to show the variation for different pairs on the same scale, we have normalized the variation in energy for each pair by its maximum value, hence all the points lie between zero and one. The solid line in each panel is the function $(1 - \cos\theta)/2$.

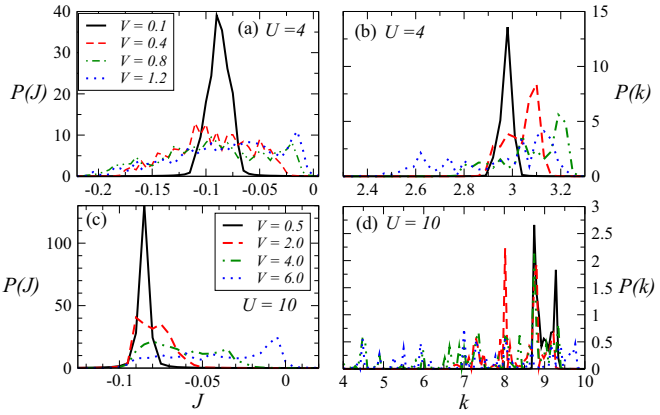

FIG. 15. Probability distributions for coupling J for (a) $U = 4$ and (c) $U = 10$ and probability distributions for amplitude stiffness k for (b) $U = 4$ and (d) $U = 10$ at various disorders.

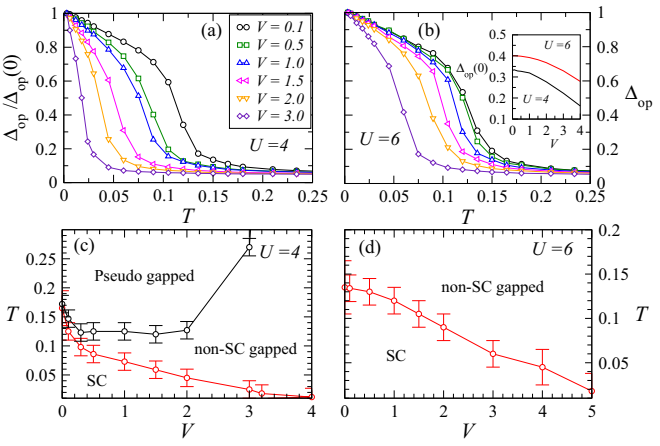

FIG. 16. Temperature dependence of the superconducting order parameter normalized by its low-temperature value $\Delta_{op}/\Delta_{op}(0)$ for (a) $U = 4$ and (b) $U = 6$. Inset in (b) shows the variation of $\Delta_{op}(0)$ with disorder strength V. The phase diagram in the temperature-disorder plane showing superconducting, nonsuperconducting gapped, and pseudogapped regimes for (c) $U = 4$ and (d) $U = 6$.

approximated by a cosine function. Interestingly, the deviation from the cosine behavior is large for intermediate values of U. For large V, the cosine curve passes through the scatter of points corresponding to $\delta E(\theta)$ for different nn pairs [see Figs. 14(b), 14(d), and 14(f)]. Note that the fit does not appear as good as that in the clean case (see Fig. 2) because we are not using additional fit parameter K in this case. In principle, more parameters can be introduced in H_{cl} in order to improve the model; however, our aim here is to demonstrate the working of the general scheme and therefore we leave this task of quantitative improvements for future. The results presented for the disordered case are averaged over four to ten realizations of disorder. We note that despite using only a few disorder realizations for averaging, the results are stable as large lattice sizes allow for a self-averaging even for a single realization of disorder.

The distribution of parameters is shown in Fig. 15. Both J_{ij} and k_i acquire a broad distribution for finite values of V. Interestingly, for large U the coupling strengths J_{ij} do not become larger than the disorder-free value of J. For the stiffness constant, $k_i < U$ for all values of disorder strength and U, and for all sites. The method employed here for calculating J_{ij} can also be useful in the study of quantum XY models where the common practice is to select J_{ij} from random uncorrelated distributions [43]. The Monte Carlo simulations proceed as in the case of the disorder-free Hamiltonian, except that in the present case the parameters k_i and J_{ij} of H_{cl} are site and bond dependent, respectively. From the behavior of the parameters for H_{cl} in the presence of disorder, we can already argue that the fluctuations in both the amplitude and the phase of the superconducting order parameter are enhanced by disorder. We show the results for the superconducting order parameter in Fig. 16(a). The $T = 0$ value of the order parameter decreases rapidly upon increasing V [see inset in Fig. 16(b)] [44]. The T_c decreases with increasing V for both $U = 4$ and 6. The trends for larger values of U are similar to those for $U = 6$. The behavior of the system for different values of V and T is summarized in two phase diagrams in Figs. 16(c) and 16(d). For intermediate U, the SC order is destabilized with increasing temperature, giving way to a nonsuperconducting phase with finite spectral gap. With further increase in T, the non-SC gapped phase evolves into a pseudogapped phase [see Fig. 16(c)]. This phase suggests that the cooper pairs are not very robust and are at the verge of breaking into normal electrons. For strong U, the non-SC gapped state is stable over a wider region in T-V space and the pseudogap phase does not appear.

The QMC studies on AHM in two dimensions indicate an existence of a superconductor to insulator transition (SIT) upon increasing disorder strength [45]. The critical value of V/t for $U/t = 4$ is found to lie between 3 and 4 for $n = 0.86$ [45]. The results obtained within our Monte Carlo method are consistent with the previous results. The critical value of disorder required for SIT increases with increasing U. The pseudogap region expands with increasing the strength of disorder for weak disorder, and reduces upon further increasing the disorder.

VI. CONCLUSIONS

We have introduced an effective Hamiltonian based Monte Carlo method for studying disordered AHM. The method is inspired by the ideas presented by Hubbard in Ref. [46] in the context of repulsive Hubbard model. The interacting Hamiltonian is replaced by (i) an effective classical Hamiltonian that controls the fluctuations of the auxiliary fields and (ii) a Hamiltonian describing electrons in arbitrary potential arising due to the auxiliary field configurations. The parameters of the classical Hamiltonian are determined from the behavior of energy variation about the BdG mean-field solutions. The results presented for the disorder-free Hamiltonian are quantitatively close to those reported in studies utilizing more sophisticated methods, such as QMC, DMFT, and SAF-MC. The effective Hamiltonian approach also provides additional insights into the behavior of the AHM. The distribution of the auxiliary fields and their evolution with U and T aid in understanding the nature of the finite temperature phase transitions. We find that while the small-U (large-U) limit is dominated by amplitude

(phase) fluctuations as expected in the BCS (BEC) scenario, both amplitude and phase fluctuations contribute significantly to the thermally induced suppression of superconductivity in the intermediate-U regime. The pseudogap phase exists in this regime just above T_c when both amplitude and phase fluctuations are active. This agrees well with the recent experimental findings in NbN superconductors. The key advantage is that a purely classical Monte Carlo method can be employed to generate auxiliary field configurations at finite temperatures. Accessibility of large lattice sizes makes this a powerful method to study the effect of disorder on superconductivity. To this end, we demonstrate that the method can indeed be used for disordered Hamiltonians. The parameters of the effective Hamiltonian become site and bond dependent in the presence of quenched disorder. The effect of disorder is to enhance fluctuations in both the amplitude and phase variables. The observation of the pseudogap in disordered s -wave superconductors is consistent with our inference that the pseudogap state is an indicator for the presence of fluctuations in both phase and amplitude of Δ_i. It should be noted that, in the disordered case, our method for computing the parameters of the classical Hamiltonian works only in the intermediate- to large-U regime. Identifying a new method to compute bond-dependent stiffness parameters J_{ij} in the small-U regime can further improve the scope of application of the general method proposed here. It will be interesting to explore the extension of our scheme to include superconducting phases with nontrivial order-parameter symmetries such as d-wave, s^{++}/s^{+-}-wave, etc. The general idea of building an effective Hamiltonian by analyzing the change in energy about the BdG mean-field state should work, provided one can identify the relevant auxiliary fields that describe the low-energy fluctuations.

ACKNOWLEDGMENTS

S.K. is grateful to T. V. Ramakrishnan for discussions and for pointing out Ref. [46]. The calculations were performed using the High Performance Computing Facility at Indian Institute of Science Education and Research Mohali. K.P. acknowledges support via a University Grants Commission fellowship. S.K. acknowledges support from Department of Science and Technology, India.

[1] R. Micnas, J. Ranninger, and S. Robaszkiewicz, Rev. Mod. Phys. **62**, 113 (1990).
[2] B. L. Gyorffy, J. B. Staunton, and G. M. Stocks, Phys. Rev. B **44**, 5190 (1991).
[3] N. Tsuji, T. Oka, P. Werner, and H. Aoki, Phys. Rev. Lett. **106**, 236401 (2011).
[4] J. E. Hirsch, Phys. Rev. Lett. **54**, 1317 (1985).
[5] Y. Wang and A. H. MacDonald, Phys. Rev. B **52**, R3876(R) (1995).
[6] W. P. Su and Y. Chen, Phys. Rev. B **64**, 172507 (2001).
[7] Z.-J. Yao, W.-Q. Chen, Y.-k. Li, G.-h. Cao, H.-M. Jiang, Q.-E. Wang, Z.-a. Xu, and F.-C. Zhang, Phys. Rev. B **86**, 184515 (2012).
[8] M. Arikawa, I. Maruyama, and Y. Hatsugai, Phys. Rev. B **82**, 073105 (2010).
[9] A. Erez and Y. Meir, Phys. Rev. Lett. **111**, 187002 (2013).
[10] A. Erez and Y. Meir, Phys. Rev. B **88**, 184510 (2013).
[11] T. Kaneko and Y. Ohta, J. Phys. Soc. Jpn. **83**, 024711 (2014).
[12] J. N. Fuchs, A. Recati, and W. Zwerger, Phys. Rev. Lett. **93**, 090408 (2004).
[13] J. K. Freericks, Phys. Rev. B **48**, 3881 (1993).
[14] E. Burovski, E. Kozik, N. Prokof'ev, B. Svistunov, and M. Troyer, Phys. Rev. Lett. **101**, 090402 (2008).
[15] S. Simonucci and G. C. Strinati, Phys. Rev. B **89**, 054511 (2014).
[16] A. Spuntarelli, P. Pieri, and G. C. Strinati, Phys. Rev. Lett. **99**, 040401 (2007).
[17] E. Zhao and A. Paramekanti, Phys. Rev. Lett. **97**, 230404 (2006).
[18] R. T. Scalettar, E. Y. Loh, J. E. Gubernatis, A. Moreo, S. R. White, D. J. Scalapino, R. L. Sugar, and E. Dagotto, Phys. Rev. Lett. **62**, 1407 (1989).
[19] N. Sakumichi, Y. Nishida, and M. Ueda, Phys. Rev. A **89**, 033622 (2014).
[20] S. Allen and A.-M. S. Tremblay, Phys. Rev. B **64**, 075115 (2001).
[21] N. Dupuis, Phys. Rev. B **70**, 134502 (2004).
[22] S. H. Pan, J. P. O'Neal, R. L. Badzey, C. Chamon, H. Ding, J. R. Engelbrecht, Z. Wang, H. Eisaki, S. Uchida, A. K. Gupta, K. W. Ng, E. W. Hudson, K. M. Lang, and J. C. Davis, Nature (London) **413**, 282 (2001).
[23] T. Cren, D. Roditchev, W. Sacks, and J. Klein, Europhys. Lett. **54**, 84 (2001).
[24] Y. Dubi, Y. Meir, and Y. Avishai, Nature (London) **449**, 876 (2007).
[25] D. Sherman, U. S. Pracht, B. Gorshunov, S. Poran, J. Jesudasan, M. Chand, P. Raychaudhuri, M. Swanson, N. Trivedi, A. Auerbach, M. Scheffler, A. Frydman, and M. Dressel, Nat. Phys. **11**, 188 (2015).
[26] B. Cheng, L. Wu, N. J. Laurita, H. Singh, M. Chand, P. Raychaudhuri, and N. P. Armitage, Phys. Rev. B **93**, 180511 (2016).
[27] S. Tarat and P. Majumdar, Eur. Phys. J. B **88**, 68 (2015).
[28] A. Ghosal, M. Randeria, and N. Trivedi, Phys. Rev. B **65**, 014501 (2001).
[29] E. W. Carlson, S. A. Kivelson, V. J. Emery, and E. Manousakis, Phys. Rev. Lett. **83**, 612 (1999).
[30] T. Paiva, R. R. dos Santos, R. T. Scalettar, and P. J. H. Denteneer, Phys. Rev. B **69**, 184501 (2004).
[31] S. Kumar and P. Majumdar, Eur. Phys. J. B **50**, 571 (2006).
[32] L. Covaci, F. M. Peeters, and M. Berciu, Phys. Rev. Lett. **105**, 167006 (2010).
[33] A. Mukherjee, N. D. Patel, C. Bishop, and E. Dagotto, Phys. Rev. E **91**, 063303 (2015).
[34] M. J. Calderón and L. Brey, Phys. Rev. B **58**, 3286 (1998).
[35] S. Kumar and P. Majumdar, Eur. Phys. J. B **46**, 315 (2005).
[36] A. Toschi, M. Capone, and C. Castellani, Phys. Rev. B **72**, 235118 (2005).
[37] D. J. Scalapino, S. R. White, and S. Zhang, Phys. Rev. B **47**, 7995 (1993).
[38] A. Erez and Y. Meir, Europhys. Lett. **91**, 47003 (2010).
[39] M. Keller, W. Metzner, and U. Schollwöck, Phys. Rev. Lett. **86**, 4612 (2001).

[40] J. J. Deisz, D. W. Hess, and J. W. Serene, Phys. Rev. B **66**, 014539 (2002).
[41] T. Paiva, R. Scalettar, M. Randeria, and N. Trivedi, Phys. Rev. Lett. **104**, 066406 (2010).
[42] B. Sacépé, C. Chapelier, T. I. Baturina, V. M. Vinokur, M. R. Baklanov, and M. Sanquer, Nat. Commun. **1**, 140 (2010).
[43] M. Swanson, Y. L. Loh, M. Randeria, and N. Trivedi, Phys. Rev. X **4**, 021007 (2014).
[44] S. Kumar and P. B. Chakraborty, Eur. Phys. J. B **88**, 69 (2015).
[45] R. T. Scalettar, N. Trivedi, and C. Huscroft, Phys. Rev. B **59**, 4364 (1999).
[46] J. Hubbard, Phys. Rev. B **19**, 2626 (1979).